


## Article

# Performance of Multilayer Composite Hollow Membrane in Separation of CO<sub>2</sub> from CH<sub>4</sub> in Mixed Gas Conditions

Shahidah Zakariya <sup>1,2</sup>, Yin Fong Yeong <sup>1,2,\*</sup>, Norwahyu Jusoh <sup>1,2</sup> and Lian See Tan <sup>3</sup> 

<sup>1</sup> Chemical Engineering Department, Universiti Teknologi PETRONAS, Seri Iskandar 32610, Perak, Malaysia; shahidah.zakariya@utp.edu.my (S.Z.); norwahyu.jusoh@utp.edu.my (N.J.)

<sup>2</sup> CO<sub>2</sub> Research Centre (CO<sub>2</sub>RES), R&D Building, Universiti Teknologi PETRONAS, Seri Iskandar 32610, Perak, Malaysia

<sup>3</sup> Department of Chemical Process Engineering, Malaysia-Japan International Institute of Technology (MJIIT), Universiti Teknologi Malaysia (UTM), Jalan Sultan Yahya Petra, Kuala Lumpur 54100, Malaysia; tan.liansee@utm.my

\* Correspondence: yinfong.yeong@utp.edu.my

**Abstract:** Composite membranes comprising NH<sub>2</sub>-MIL-125(Ti)/PEBAX coated on PDMS/PSf were prepared in this work, and their gas separation performance for high CO<sub>2</sub> feed gas was investigated under various operating circumstances, such as pressure and CO<sub>2</sub> concentration, in mixed gas conditions. The functional groups and morphology of the prepared membranes were characterized by Fourier transform infrared spectroscopy (FTIR) and field emission scanning electron microscopy (FESEM). CO<sub>2</sub> concentration and feed gas pressure were demonstrated to have a considerable impact on the CO<sub>2</sub> and CH<sub>4</sub> permeance, as well as the CO<sub>2</sub>/CH<sub>4</sub> mixed gas selectivity of the resultant membrane. As CO<sub>2</sub> concentration was raised from 14.5 vol % to 70 vol %, a trade-off between permeance and selectivity was found, as CO<sub>2</sub> permeance increased by 136% and CO<sub>2</sub>/CH<sub>4</sub> selectivity reduced by 42.17%. The membrane produced in this work exhibited pressure durability up to 9 bar and adequate gas separation performance at feed gas conditions consisting of high CO<sub>2</sub> content.

**Keywords:** dip-coating; metal organic frameworks (MOFs); multilayer composite hollow fiber membrane; CO<sub>2</sub>/CH<sub>4</sub> mixed gas separation



**Citation:** Zakariya, S.; Yeong, Y.F.; Jusoh, N.; Tan, L.S. Performance of Multilayer Composite Hollow Membrane in Separation of CO<sub>2</sub> from CH<sub>4</sub> in Mixed Gas Conditions. *Polymers* **2022**, *14*, 1480. <https://doi.org/10.3390/polym14071480>

Academic Editor: Zina Vuluga

Received: 11 February 2022

Accepted: 12 March 2022

Published: 5 April 2022

**Publisher's Note:** MDPI stays neutral with regard to jurisdictional claims in published maps and institutional affiliations.



**Copyright:** © 2022 by the authors. Licensee MDPI, Basel, Switzerland. This article is an open access article distributed under the terms and conditions of the Creative Commons Attribution (CC BY) license (<https://creativecommons.org/licenses/by/4.0/>).

## 1. Introduction

Natural gas is a more desirable power source than coal since it has a lower carbon impact [1,2]. Natural gas usually contains 50% to 90% methane (CH<sub>4</sub>); nevertheless, harmful contaminants such as water (H<sub>2</sub>O), carbon dioxide (CO<sub>2</sub>), hydrogen sulfide (H<sub>2</sub>S), nitrogen (N<sub>2</sub>), ethane (C<sub>2</sub>H<sub>6</sub>), propane (C<sub>3</sub>H<sub>8</sub>), and toluene are often found in unprocessed natural gas [3]. With the presence of H<sub>2</sub>O, the acid gases CO<sub>2</sub> and H<sub>2</sub>S may damage the processing and transportation equipment; thus, raw natural gas must be treated before use [4,5]. In many petroliferous basins, especially in Southeast Asia, high carbon dioxide levels in reservoirs make exploration challenging. The offshore field in Malay Basin's reservoir usually poses high CO<sub>2</sub> concentrations, making exploration difficult. Some fields contain more than 80% CO<sub>2</sub>, making them undesirable development prospects [6].

CO<sub>2</sub> removal is crucial in the natural gas purification process. It causes corrosion in pipelines, lowers the calorific value of natural gas, and raises maintenance and operating costs [7]. For the past few decades, membrane technology has reigned supreme in gas separation processes due to its low cost and ease of processing [8,9]. However, the trade-off between permeability and selectivity limits the gas separation performance of the commercially used polymeric materials [10].

Progress in polymeric materials for gas separation has accelerated dramatically in the past few decades, including polysulfone (PSf), cellulose acetate (CA), polyethersulfone (PES), and the polyimide family [11]. PSf has been widely explored and used for membrane

separation among polymeric materials due to its lower material cost and suitable mechanical strength, thermal stability, chemical stability, and gas permeation [12]. However, the well-known “trade-off” between permeability and selectivity caused by the formation of defects, such as the presence of macrovoids on the fiber surface, has resulted in poor gas selectivity [8,9].

To overcome these limitations, various techniques have been proposed, including polymer blending, ultraviolet-assisted graft polymerization, plasma-induced graft polymerization, incorporation of fillers into polymer membrane matrix, and a caulking technique that involves coating the defective membrane skin with highly permeable polymers [13,14]. Surface coating, which is typically coated on porous membrane supports with a highly permeable gutter layer and a selective layer, is one of the most effective ways to improve membrane performance in gas separation [15].

Dip-coating is a popular technique for producing thin-film composite hollow fiber membranes. Thin-film composite membranes with several layers are being developed for use in gas separation applications to enhance the efficiency of thin-film composite membranes. To cover existing flaws and protect the selective layer from abrasion or harmful chemical assaults, the protective layer is usually applied on top of the selective layer [16]. On the substrate surface, the gutter layer is applied to enhance adhesion between the selected selective layer and substrate. Additionally, the gutter layer may help to reduce mass transport resistance since it is usually constructed of highly permeable materials [17].

The gutter layer acts as a bridge between the hollow fiber substrate and the selective layer, while the ultra-thin selective layer separates the gases [18]. It is typical to utilize the Polydimethylsiloxane (PDMS) coating as a gutter layer to smooth the surface, close the macrovoid, and prevent polymers from penetrating into the porous substrate [15]. However, PDMS coatings suffer from low surface energy that can cause poor interfacial adhesion between the gutter layer and the selective layer [19]. As an alternative, a composite selective layer containing inorganic fillers was incorporated into the membrane matrix to improve gas permeability [15]. Typically, rubbery-type polymers are employed because of their softness and flexibility, as well as their controlled gas penetration characteristics due to their solubility selectivity [20]. Many researchers utilize poly(ethylene oxide) (PEO) among various rubbery materials instead of PDMS since it has been identified as the preferable chemical group that interacts effectively with CO<sub>2</sub> [17,18].

Polyether block amide (PEBAX) is a commercially available copolymer composed of polyamide and PEO that is well suited for use as a selective layer material. The benefits of this polymer include high skin formation ability and solvent resistance [21]. Chen et al. used the dip-coating method to prepare PEBA/PDMS/PAN multilayer composite hollow fiber membranes (HFMs) for flue gas treatment. Coating parameters such as polymer content and coating duration were studied, and they found that CO<sub>2</sub> permeance of the composite membranes was improved [20].

On the other hand, over the years, many efforts have been undertaken to develop mixed matrix membranes (MMMs) for gas separation in order to overcome the limitations of polymeric materials. Lately, an MMM consisting of a new type of inorganic filler, metal organic frameworks (MOF), has been widely reported. This type of filler exhibits excellent interaction with polymers owing to its organic linkers and open metal sites [22]. One of the MOF species that shows high porosity is functionalized titanium, also known as NH<sub>2</sub>-MIL-125(Ti). In a recent work, Nadia Hartini et al. (2020) incorporated NH<sub>2</sub>-MIL-125(Ti) into a 6FDA-durene polymer matrix for CO<sub>2</sub>/CH<sub>4</sub> separation. Membranes loaded with 7.0 wt.% of filler showed the highest CO<sub>2</sub> permeability and CO<sub>2</sub>/CH<sub>4</sub> selectivity, surpassing the 2008 Robeson upper bound [23]. Similarly, Waqas Anjum et al. found that although employing both MIL-125 and NH<sub>2</sub>-MIL-125(Ti) fillers enhances overall separation performance, the NH<sub>2</sub>-functionalized filler is recommended since it leads to better selectivity and permeability [24].

In our previous work, we investigated single gas performance of a series of composite membranes containing different compositions of NH<sub>2</sub>-MIL-125(Ti) in PEBAX, coated on

a PSf hollow fiber support layer [25]. Enhancement of CO<sub>2</sub> and CH<sub>4</sub> gas permeance was discovered for composite membranes when compared to the PSf membranes coated only with PDMS or PEBAX solutions. Furthermore, the largest increment in CO<sub>2</sub>/CH<sub>4</sub> ideal selectivity was found for a composite membrane loaded with 10% of NH<sub>2</sub>-MIL-125(Ti) filler [25]. The key reasons for the improvement in CO<sub>2</sub> removal from CH<sub>4</sub> are the high porosity and strong CO<sub>2</sub> affinity of NH<sub>2</sub>-MIL-125(Ti) filler [25].

Currently, most of the research on membrane development is concentrated on single gas permeation and draws conclusions about membrane performance based on these data. This technique may cause inaccurate results owing to the lack of impurities and multicomponent gas effects, which greatly degrade pure gas performance [26].

Significant research has been conducted throughout the past few decades, with an emphasis on the modification of various polymeric precursors in the formation of hollow fiber membranes and evaluation of the resultant fibers in single gas permeation. In contrast, relatively few literature works concentrate on binary gas separation [27]. Hence, in this work, we further explore the performance of our previously developed composite hollow fiber membrane in CO<sub>2</sub>/CH<sub>4</sub> separation in mixed gas conditions at various operating conditions such as CO<sub>2</sub> feed concentration and pressure. Although in real natural gas purification processing, other impurities are present in the feed stream, the performance of the membrane in CO<sub>2</sub> and CH<sub>4</sub> binary gas mixture separation still could serve as the initial performance indicator prior to upscaling the membrane in real gas separation conditions [28].

## 2. Materials and Methods

### 2.1. Chemicals and Materials

Polysulfone, Mw 35,000 supplied from Sigma-Aldrich (St. Louis, MO, USA), was utilized as the polymer matrix phase for the creation of the hollow fiber membrane substrate. N,N-dimethylacetamide (DMAc), ethanol, and tetrahydrofuran (THF) were supplied by Merck and used as received. Polydimethylsiloxane (PDMS) coating layer was supplied by Sigma-Aldrich (St. Louis, MO, USA). Hexane supplied by Merck (Darmstadt, Germany) was utilized as the solvent in the preparation of PDMS coating solutions. Commercial PEBAX MH-1657 polymer was purchased from Arkema Group (Colombes, France). Previously self-synthesized NH<sub>2</sub>-MIL-125(Ti) particles were used as fillers [23].

### 2.2. Fabrication of PSf Hollow Fiber Substrates

The formula for preparing the dope solution is described in detail in our previous work [25]. With the dry/wet spinning process, PSf hollow fiber was spun using a spinneret with dimensions of OD/ID of 0.80 mm/0.4 mm at an air gap distance of 3.0 cm, while the take-up speed was maintained at 5.0 rpm. Then, fibers were immersed in water to remove the solvent residue for three days. Wetted fibers were then washed three times with methanol and n-hexane for 30 min each time. The solvent-exchanged fibers were then dried at room temperature before being subjected to characterization and gas permeation experiments [29].

### 2.3. Preparation of Gutter Layer and Selective Layer

The coating solution of the gutter layer was prepared by stirring 3 wt.% PDMS in n-hexane. The coating solution of the selective layer was prepared by dissolving PEBAX pellets in a 70/30 ethanol/water solvent mixture at a concentration of 2%. The mixture was agitated under reflux at 85 °C for approximately 2 h until it was fully dissolved, and then a 5–20 wt.% loading of NH<sub>2</sub>-MIL-125(Ti) particles synthesized in our previous work (surface area of 1205.9 m<sup>2</sup> g<sup>-1</sup> and pore volume of 0.53 cm<sup>3</sup> g<sup>-1</sup>) [23] was added to the solution. Prior to coating, the NH<sub>2</sub>-MIL-125(Ti)/PEBAX suspension was alternately stirred and sonicated for 30 min to ensure complete dispersion of particles in the solution. Subsequently, this solution was stirred and sonicated again to remove any bubbles formed prior to coating. The hollow fiber membranes were first dip-coated for 10 min with PDMS solution as a

gutter layer. Then, the coated hollow fibers were dried for 24 h before being coated with NH<sub>2</sub>-MIL-125(Ti)/PEBAX solution. Finally, the composite hollow fibers were cured at room temperature for 48 h before proceeding to gas separation testing. The membranes developed in our previous work [25] and used in this study are shown in Table 1.

**Table 1.** Membranes prepared in our previous work [25] used in this study.

Code	Multiplayer Composite Membranes	Filler Loading (%)
C	PSf/PDMS	0
C <sub>0</sub>	PSf/PDMS/PEBAX	0
C <sub>5</sub>	PSf/PDMS/PEBAX-NH <sub>2</sub> -MIL-125(Ti)-5wt.%	5
C <sub>10</sub>	PSf/PDMS/PEBAX-NH <sub>2</sub> -MIL-125(Ti)-10wt.%	10
C <sub>15</sub>	PSf/PDMS/PEBAX-NH <sub>2</sub> -MIL-125(Ti)-15wt.%	15
C <sub>20</sub>	PSf/PDMS/PEBAX-NH <sub>2</sub> -MIL-125(Ti)-20wt.%	20

#### 2.4. Characterization of Hollow Fiber Membranes

The crystallinity of all composite membranes was examined by using an X-ray diffractometer (X'Pert3 Powder, Panalytical, Malvern, UK) with Cu K $\alpha$  radiation at ambient temperature. The surface of each hollow fiber sample was irradiated with X-rays and the intensities and scattering angles of the X-rays that leave the samples were measured from 2 $\theta$  values of 5° to 35°. In addition, attenuated total reflectance (ATR)-FTIR was used to acquire infrared spectra of the resulting membranes. A total of 50 scans with wavenumbers ranging from 650 to 4000 cm<sup>-1</sup> were used to obtain the spectrum of the outer surface of each hollow fiber membrane with a sample size of 1 cm. The morphology of hollow fiber membranes was examined by field emission scanning electron microscopy (FESEM) using a Zeiss Supra 55VP (Jena, Germany). The membrane surface was analyzed for elemental composition using a dispersive X-ray spectrometer (EDS), Bruker Quantax 70 (Berlin, Germany), to confirm the presence of Ti in the NH<sub>2</sub>-MIL-125(Ti) particle in the coating layer.

#### 2.5. CO<sub>2</sub>/CH<sub>4</sub> Binary Gas Separation Testing

The module was produced by assembling a few 9 cm long fibers prior to the mixed gas permeation test, as illustrated in Figure 1. Both sides of the module were sealed using a 5 min high-performance epoxy glue that was then allowed to dry for 24 h. The module was then placed in a stainless steel pressure chamber for the gas separation test. The binary gas permeability of the resulting membrane was tested from 1 to 9 bar using CO<sub>2</sub>/CH<sub>4</sub> binary mixtures containing 14.5 vol %, 42.5 vol %, and 70.0 vol % of CO<sub>2</sub>. Gas chromatography (Perkin Elmer, model GCNARL9680, Waltham, MA, USA) equipped with a thermal conductivity detector (TCD) was used to evaluate the gas compositions of feed, retentate, and permeate gas streams. The full experimental and set-up methods have been published elsewhere [30]. The permeability of each gas was calculated by using Equations (1) and (2), which are as follows [31]:

$$P_{\text{CO}_2} = \frac{V_p y_{\text{CO}_2} t}{A_m (P_h x_{\text{CO}_2} - P_l y_{\text{CO}_2})} \quad (1)$$

$$P_{\text{CH}_4} = \frac{V_p y_{\text{CH}_4} t}{A_m (P_h x_{\text{CH}_4} - P_l y_{\text{CH}_4})} \quad (2)$$

where  $P_{\text{CO}_2}$ ,  $V_p$ ,  $A_m$ ,  $P_h$ ,  $P_l$ ,  $x$ , and  $y$  are CO<sub>2</sub> permeability (GPU) in the gas mixture, permeate flow rate (cm<sup>3</sup>(STP)/s), membrane area (cm<sup>2</sup>), feed pressure (bar), permeate pressure (bar), and the mole fractions of the component in the feed and permeate streams, respectively. The same equations were used to determine the CH<sub>4</sub> permeability in the gas mixture.

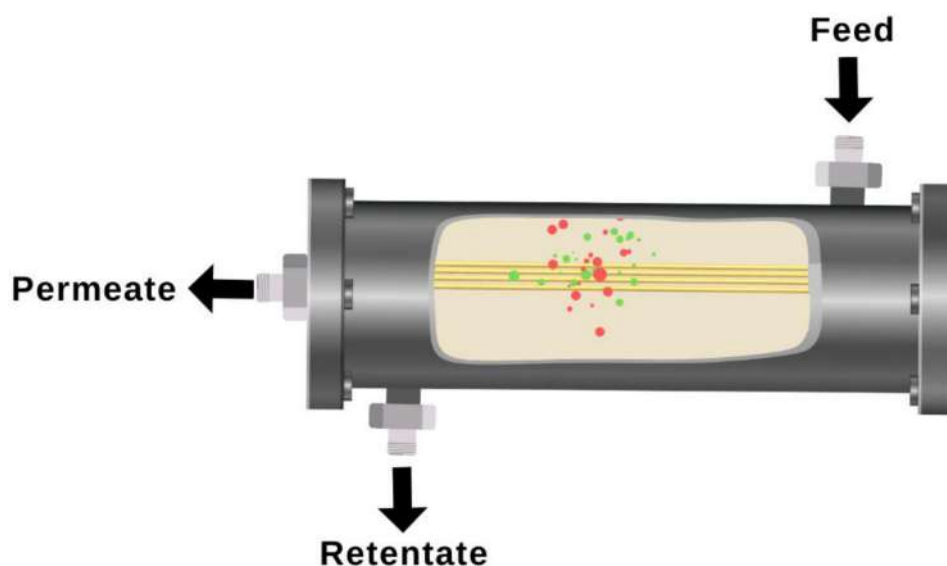


**Figure 1.** Schematic diagram of the gas permeation test module.

The  $\text{CO}_2/\text{CH}_4$  mixed gas selectivity was calculated using Equation (3) as follows [32]:

$$\alpha_{\text{CO}_2/\text{CH}_4} = \frac{y_{\text{CO}_2}y_{\text{CH}_4}}{x_{\text{CO}_2}x_{\text{CH}_4}} \quad (3)$$

### 3. Results and Discussion

#### 3.1. X-ray Diffraction (XRD)

The X-ray diffraction patterns of the resulting membranes are shown in Figure 2. Normally, a polymer sample with an amorphous region exhibits a wide peak intensity [33]. From the results obtained, the XRD pattern for almost all hollow fiber membranes showed a wide band between  $15^\circ$  and  $20^\circ$ . By embedding the particles in the polymer matrix, the membranes became more amorphous, and this result is consistent with the previous results described by Ghasemi et al. [34]. Moreover, the membranes' broad peaks were attributed to the compatibility and full homogeneity of membrane components [35]. Following the integration of the MOFs, the peak locations remained unchanged, demonstrating that there were no changes in the d-spacing of the polymer [27].

#### 3.2. Fourier Transform Infrared Spectroscopy (FTIR)

Figure 3 shows the FTIR spectra of PSf hollow fiber membranes coated with PDMS, PEBAX, and  $\text{NH}_2\text{-MIL-125(Ti)/PEBAX}$  containing 5, 10, 15, and 20 wt.%  $\text{NH}_2\text{-MIL-125(Ti)}$  particles. The FTIR spectrum of  $\text{NH}_2\text{-MIL-125(Ti)}$  shows a broad peak between  $3400$  and  $3700\text{ cm}^{-1}$ , ascribed to  $-\text{NH}_2$ 's stretching vibration [36]. Peaks between  $1658$  and  $1253\text{ cm}^{-1}$  shown by  $\text{NH}_2\text{-MIL-125(Ti)}$  fillers correspond to carboxylic acid functional groups within the MOF structure [37]. Meanwhile, asymmetric stretching vibration bands at  $1654\text{ cm}^{-1}$  ( $\text{C}=\text{O}$ ) and symmetric stretching vibration bands at  $1253\text{ cm}^{-1}$  ( $\text{C}-\text{O}$ ) observed in the spectrum are attributed to the presence of carbonyl groups in the filler [38]. Peaks between  $500$  and  $800\text{ cm}^{-1}$  are attributed to the  $\text{O-Ti-O}$  vibration [39]. These remarkable peaks demonstrate the successful synthesis of  $\text{NH}_2\text{-MIL-125(Ti)}$ . On the other hand, a band at  $793\text{ cm}^{-1}$  shown in the FTIR spectrum of PDMS/PSf membrane (C) corresponds to the stretching vibration of  $\text{Si-O}$  bonds. The presence of this band in the FTIR spectrum indicates the presence of PDMS sub-chains in the membrane [40]. Additionally, peaks at  $2966$ ,  $1102$ , and  $1014\text{ cm}^{-1}$  shown in the PDMS/PSf (C) spectrum correspond to the  $\text{C-H}$  stretching vibrations of  $\text{Si-CH}_3$  and  $\text{Si-O-Si}$  [41].

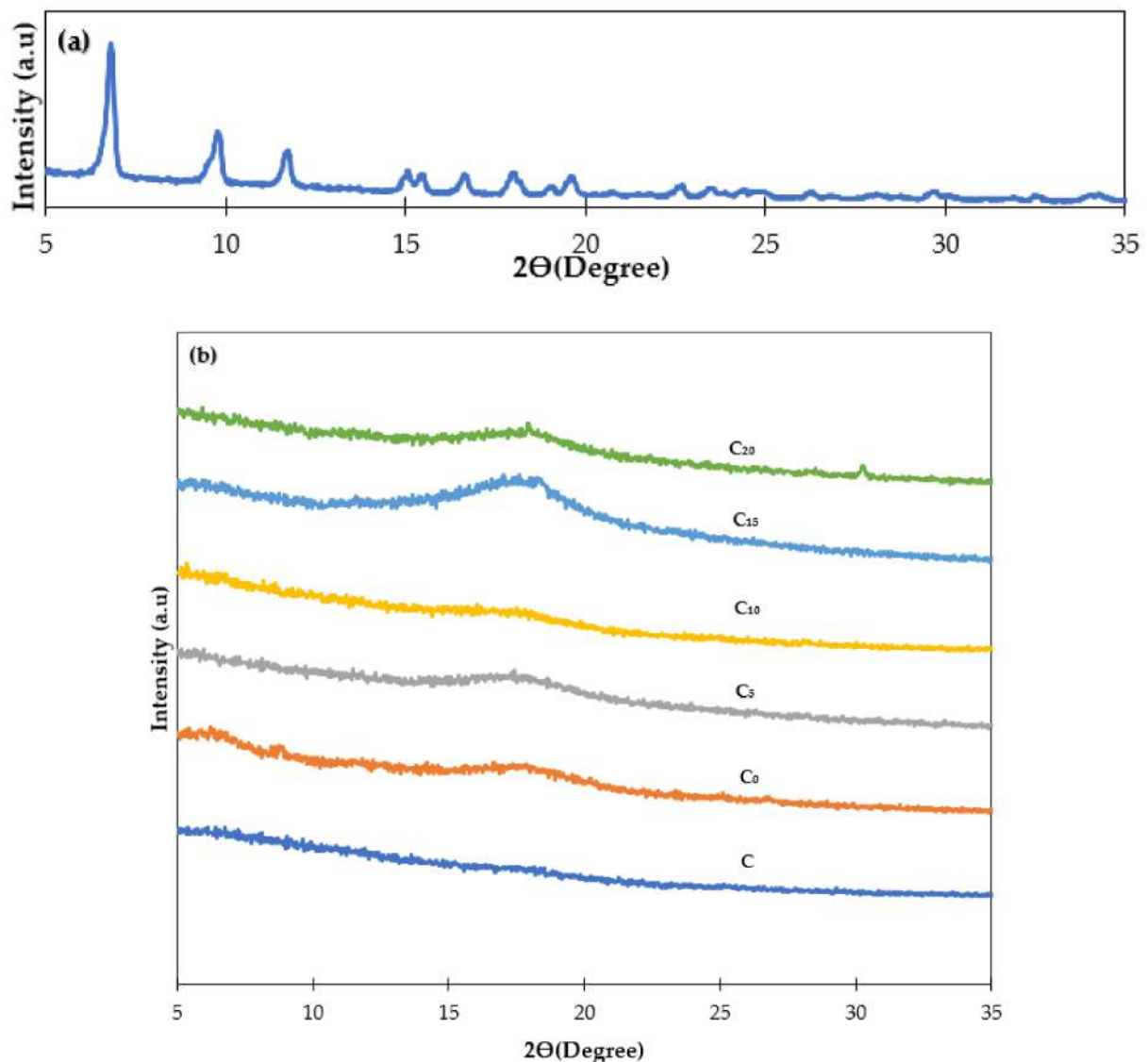


**Figure 2.** XRD patterns of (a)  $\text{NH}_2\text{-MIL-125(Ti)}$  and (b) composite membranes.

For the PEBAX/PDMS/PSf ( $\text{C}_0$ ) membrane, the distinct peak at around  $1238\text{ cm}^{-1}$  is attributed to the stretching vibration of the C–O–C group within the PEO segment [42]. Furthermore, the membrane exhibits relatively sharp peaks at  $3301$ ,  $1488$ , and  $1641\text{ cm}^{-1}$ . These peaks are attributed to the hard polyamide segment's –N–H–, H–N–C=O, and O–C=O groups [42]. Referring to Figure 3, membranes  $\text{C}_5\text{-C}_{20}$  exhibit minor bands from  $3400$  to  $3700\text{ cm}^{-1}$ , corresponding to the – $\text{NH}_2$  stretching vibration from the particles. Considering this, the bands associated with the PEBAX selective layer are stronger, indicating that the PDMS bands detected might be caused by the PEBAX layer.

It can be seen from Figure 3 that membranes  $\text{C}_0\text{-C}_{20}$  exhibit similar FTIR spectra. However, in comparison with the  $\text{C}_0$  membrane, the reduced peak at  $1253\text{ cm}^{-1}$  in the FTIR spectrum of the membrane  $\text{C}_{10}$  indicates the interaction of PEBAX and  $\text{NH}_2\text{-MIL-125(Ti)}$ . This observation shows that the  $\text{NH}_2\text{-MIL-125(Ti)}$  particles on the surface of fibers disturbed the chain of PEBAX. Additionally, no new peaks were found in the FTIR spectra of composite membranes ( $\text{C}_5\text{-C}_{20}$ ), indicating that the  $\text{NH}_2\text{-MIL-125(Ti)}$  and PEBAX were physically blended [43].

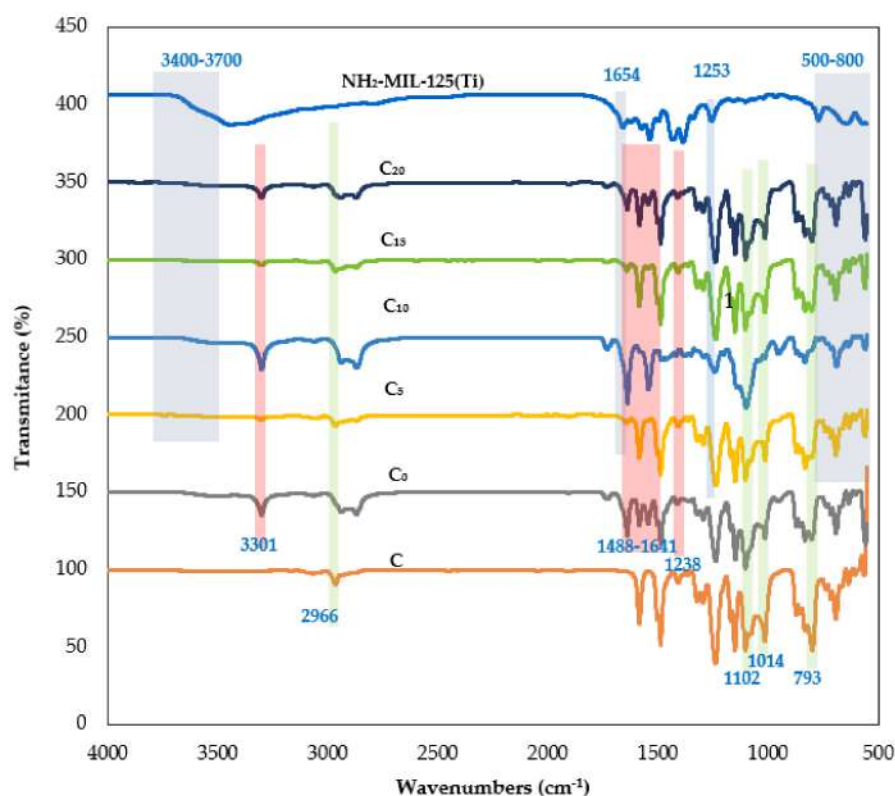


**Figure 3.** FTIR spectra of fillers and composite hollow fiber membranes.

### 3.3. Field Emission Scanning Electron Microscopy (FESEM)

Figure 4 shows the FESEM images of PSf/PDMS membrane (C) at the outer surface. The outer surface of the membrane after PDMS coating became denser and smoother. This may help eliminate the solution intrusion during the subsequent coating of the selective layer containing  $\text{NH}_2\text{-MIL-125(Ti)}$  in PEBAX.

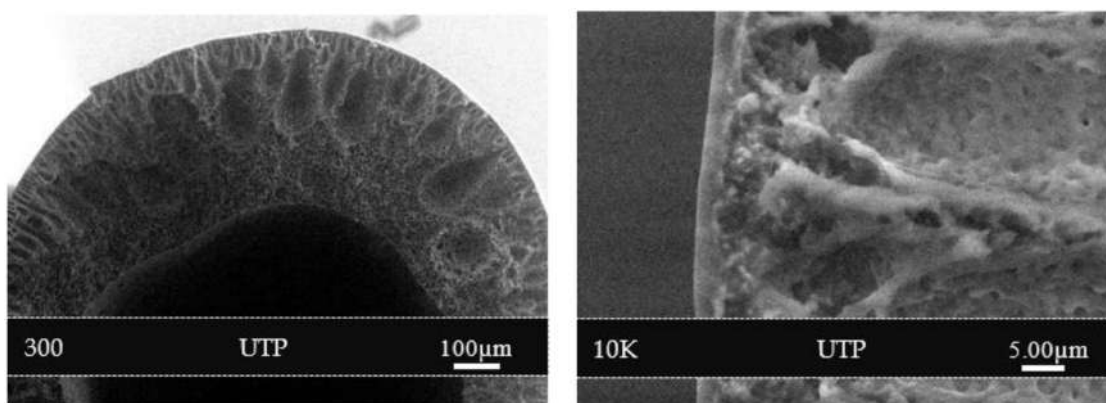


**Figure 4.** Cross-section morphology of PSf/PDMS membrane (C) at 300 and 10 K magnifications.

The outer skin, which is composed of a PEBAX/ $\text{NH}_2\text{-MIL-125(Ti)}$  selective layer at various filler loadings, is responsible for gas separation, whereas the porous sublayer beneath offers both mechanical support and separation [9]. FESEM images of the PSf hollow fiber coated with PDMS as the first layer and  $\text{NH}_2\text{-MIL-125(Ti)}$ /PEBAX as a subsequent layer are shown in Figure 5. From Figure 5, it can be seen that a modest particle dispersion with the same thickness was found for all membranes (Figure 5a–c), where the concave surface is visible and smaller particles were most likely present in the coating dispersion, leading them to adhere to the membrane surface. This is owing to the flexibility of the PEBAX chains, which enables superior contact and adhesion with the  $\text{NH}_2\text{-MIL-125(Ti)}$

particle [44]. Figure 5d shows a slight reduction in the thickness of the membrane loaded with 20%  $\text{NH}_2\text{-MIL-125(Ti)}$ . Ultimately, all the images demonstrate that the PEBAX coating layer provides a conducive environment for the adhesion of  $\text{NH}_2\text{-MIL-125(Ti)}$  particles to the membrane surface. In an earlier work, our EDX mapping analysis was performed on the membrane surface to determine the distribution of  $\text{NH}_2\text{-MIL-125(Ti)}$  particles in the outer coating layer [25]. The existence of  $\text{NH}_2\text{-MIL-125(Ti)}$  on the membrane surface was confirmed by scanning the elements of titanium, the major component of  $\text{NH}_2\text{-MIL-125(Ti)}$ . Certainly, the dispersion of titanium increased with higher particle loadings.

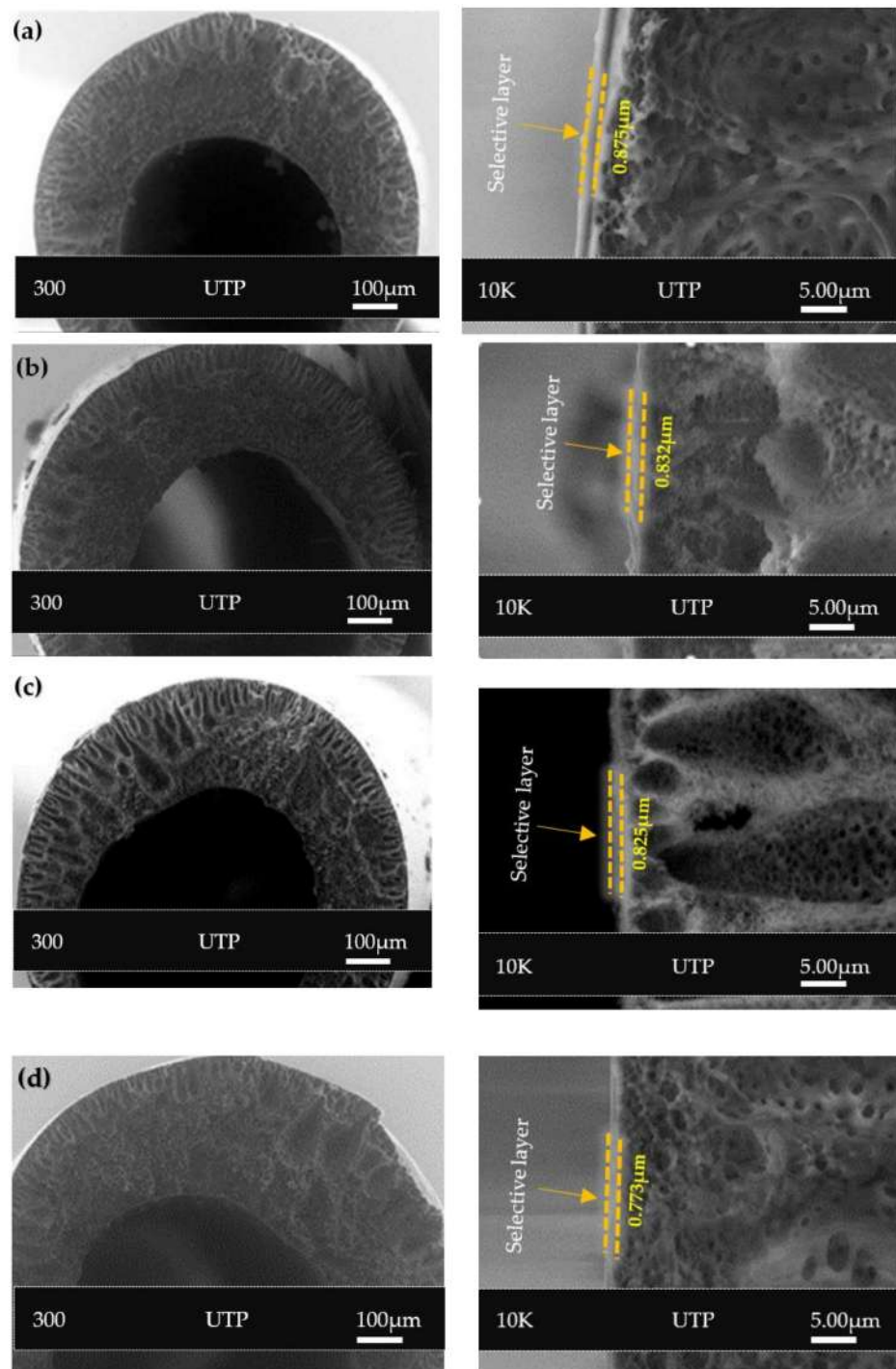


**Figure 5.** Cross-section morphology of composite hollow fiber membranes at 300 and 10 K magnifications (a) C<sub>5</sub>, (b) C<sub>10</sub>, (c) C<sub>15</sub>, and (d) C<sub>20</sub>.



### 3.4. CO<sub>2</sub>/CH<sub>4</sub> Mixed Gas Separation Performance

#### 3.4.1. Effect of CO<sub>2</sub> Concentration in Feed Stream

Our previous study found that the best single gas permeation performance was exhibited by a composite membrane loaded with 10 wt.% filler (C<sub>10</sub>) [25]. In the present work, we further explore the performance of this membrane in CO<sub>2</sub>/CH<sub>4</sub> separation in mixed gas conditions. Figure 6 shows the effect of CO<sub>2</sub> feed composition on CO<sub>2</sub> and CH<sub>4</sub> permeances as well as the selectivity in mixed gas separation evaluated at 25 °C for the C<sub>10</sub> membrane. The CO<sub>2</sub> concentrations ranged from 14.5 vol % to 70 vol % at a feed pressure of 5 bar. CO<sub>2</sub> is well known as a plasticizer for polymeric membranes. The higher the CO<sub>2</sub> content in the membrane, the greater the polymer free volume and segmental mobility, resulting in a decrease in membrane selectivity [45].

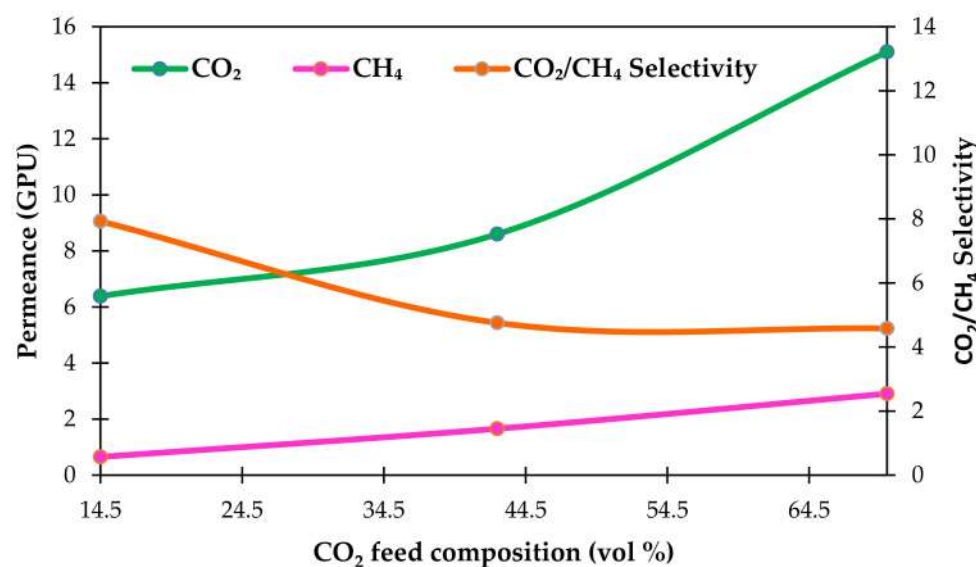


**Figure 6.** Effect of CO<sub>2</sub> feed concentration on CO<sub>2</sub> and CH<sub>4</sub> permeances and CO<sub>2</sub>/CH<sub>4</sub> mixed gas selectivity in mixed gas separation at feed pressure of 5 bar.

As seen in Figure 6, CO<sub>2</sub> permeance steadily increases as CO<sub>2</sub> concentration increases, and vice versa for membrane selectivity. At a CO<sub>2</sub> feed concentration of 70 vol %, a maximum CO<sub>2</sub> permeance of 15.10 GPU is attained. Meanwhile, with a CO<sub>2</sub> feed concentration of 14.5 vol %, a minimum CO<sub>2</sub> permeance of 6.4 GPU is attained. Furthermore, under equal operating circumstances, the CO<sub>2</sub> permeance increase is modest for CO<sub>2</sub> concentrations below 40 vol %, being around 35%, compared to that for CO<sub>2</sub> concentrations beyond 40 vol %, which is about 76%.

However, the results demonstrate that selectivity declined as CO<sub>2</sub> feed concentration increased. The CO<sub>2</sub>/CH<sub>4</sub> mixed gas selectivity showed a substantial decline from CO<sub>2</sub> feed concentrations of 14.5 vol % CO<sub>2</sub> to 70 vol % CO<sub>2</sub> (about 42%). Lower CO<sub>2</sub>/CH<sub>4</sub> mixed gas selectivity was observed at higher CO<sub>2</sub> concentrations, despite the membrane showing larger CO<sub>2</sub> adsorption potential. This phenomenon is mainly due to the greater CH<sub>4</sub> adsorption capability of the membrane, which reduced the mixed gas selectivity [44]. As a result, a maximum CO<sub>2</sub>/CH<sub>4</sub> mixed gas selectivity of 7.9 was obtained at a CO<sub>2</sub> feed concentration of 14.5 vol %. Furthermore, increasing the CO<sub>2</sub> feed concentration from 42.5 vol % to 70 vol % resulted in the saturation of the amine–CO<sub>2</sub> interaction, which aggregated CO<sub>2</sub> on the feed side of the membrane, thus lowering the CO<sub>2</sub>/CH<sub>4</sub> mixed gas selectivity [46]. Additionally, a larger CO<sub>2</sub> feed concentration might inflate the polymer matrix, resulting in an increase in the rate of CH<sub>4</sub> penetration through the membrane [47].

From the results obtained in this work, we found that the selectivity of mixed gas is less than that of pure gases [48]. However, the mixed gas selectivity of CO<sub>2</sub>/CH<sub>4</sub> is greater than the CO<sub>2</sub>/CH<sub>4</sub> ideal selectivity at a CO<sub>2</sub> feed concentration of 14.5%, indicating that CO<sub>2</sub> and CH<sub>4</sub> compete for the adsorption site in the membrane. In comparison, at

a CO<sub>2</sub> feed concentration of 70 vol %, the CO<sub>2</sub> permeance rose by 112%, up to 15.1 GPU, compared to 7.1 GPU for pure gas permeation. Moreover, CO<sub>2</sub>/CH<sub>4</sub> mixed gas selectivity reduced from 7.9 (CO<sub>2</sub> feed concentration of 14.5 vol %) to 4.6 (CO<sub>2</sub> feed concentration of 70 vol %), which is less than the CO<sub>2</sub>/CH<sub>4</sub> ideal selectivity of 11.9 obtained in our previous work [25].

### 3.4.2. Effect of Feed Pressure

We further conducted the separation experiment on the C<sub>10</sub> membrane at different pressures up to 9 bar, and Figure 7 illustrates the effect of feed pressure from 1 to 9 bar on the performance of the C<sub>10</sub> membranes at 42.5 vol % CO<sub>2</sub> feed concentration.

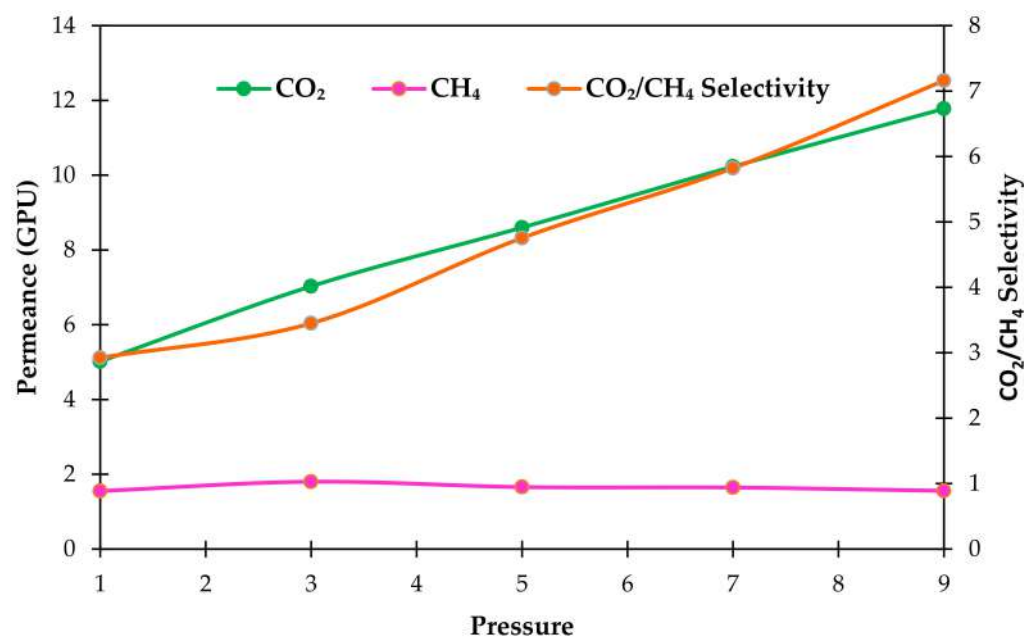


**Figure 7.** Effect of pressure on CO<sub>2</sub> and CH<sub>4</sub> permeances and CO<sub>2</sub>/CH<sub>4</sub> mixed gas selectivity in mixed gas separation at 42.5 vol % CO<sub>2</sub> feed concentration.

Referring to Figure 7, increasing the feed pressure caused the increment of CO<sub>2</sub> and CH<sub>4</sub> permeance, as well as CO<sub>2</sub>/CH<sub>4</sub> mixed gas selectivity. The maximum CO<sub>2</sub> permeance of 11.8 GPU was obtained at 9 bar. Meanwhile, at 1 bar, a minimum CO<sub>2</sub> permeance of 5.0 GPU was achieved. The CO<sub>2</sub> permeability rose 135%, from 5.0 GPU to 11.8 GPU, when the pressure was raised from 1 to 9 bar. However, a distinct pattern can be seen for the CH<sub>4</sub> permeability. It remained relatively consistent between 1.5 GPU and 1.8 GPU when the pressure increased from 1 to 9 bar. This phenomenon could be explained by greater CO<sub>2</sub> condensability as a result of its increased sorption capability.

Moreover, the increment of CO<sub>2</sub> permeance at higher pressures could be also related to the increase in gas solubility, caused by the enhancement of CO<sub>2</sub> molecule sorption in the polymeric network, where the CO<sub>2</sub> fills the gap between the polymer network's chains. This widens the distance between these bonds, and thus increases the mobility of the polymeric chain [46] and plasticizes the membrane. Eventually, the gas permeance and the gas compressibility of the membrane increase [49]. For all pressures investigated in this experiment, CO<sub>2</sub> permeance rose roughly linearly with increasing pressure, but CH<sub>4</sub> permeability decreased, showing competition for adsorption sites and, once again, preferential adsorption of CO<sub>2</sub> over CH<sub>4</sub> [50].

Furthermore, by increasing the feed pressure, CO<sub>2</sub>/CH<sub>4</sub> mixed gas selectivity was also increased. When the pressure increased from 1 to 9 bar, the selectivity increased from 2.9 to 7.2 (Figure 7). This result is mainly due to higher CO<sub>2</sub> condensability compared to CH<sub>4</sub> (T<sub>c</sub> of CO<sub>2</sub> is 31.1 °C compared to 82.3 °C for CH<sub>4</sub>), which resulted in a stronger affinity of CO<sub>2</sub> to the membrane. Moreover, the kinetic diameter of CO<sub>2</sub> of 3.3 Å is smaller

than that of CH<sub>4</sub> (3.82 Å); therefore, the penetration rate of CO<sub>2</sub> over the membrane was greater than CH<sub>4</sub> [51]. In addition, the increase in mixed gas selectivity is also due to the inherent flexibility of NH<sub>2</sub>-MIL-125(Ti) filler.

As can be seen from Figure 7, the CO<sub>2</sub> permeance and CO<sub>2</sub>/CH<sub>4</sub> mixed gas selectivity of the membrane increase with increasing feed pressure. These results reveal that satisfactory separation performance can be maintained at higher pressure. Thus, it can be deduced that the PSF/PDMS/PEBAX/NH<sub>2</sub>-MIL-125(Ti) membrane prepared in this work can be considered as a promising candidate for practical membrane-based natural gas purification.

#### 4. Conclusions

Multilayer composite hollow fiber membranes containing NH<sub>2</sub>-MIL-125(Ti) particles were fabricated using the dip-coating technique and assessed for CO<sub>2</sub>/CH<sub>4</sub> separation at various CO<sub>2</sub> feed concentrations and feed pressures. Additionally, the chemical structure, phase structure, and morphology of the membrane were studied using different analytical tools. The XRD patterns showed the typical NH<sub>2</sub>-MIL-125(Ti) structure peaks with an amorphous state in the membranes, and no crystallization of the NH<sub>2</sub>-MIL-125(Ti) was found during the coating procedure in the composite membranes. FTIR results revealed that the addition of more particles into the polymer matrix resulted in no new peaks for all the composite membranes, implying the physical blending feature of NH<sub>2</sub>-MIL-125(Ti) and within the PEBAX bulk. CO<sub>2</sub> permeance was greatest at a 70 vol % CO<sub>2</sub> feed composition, but it decreased slightly compared to single gas permeation. The highest CO<sub>2</sub>/CH<sub>4</sub> mixed gas selectivity obtained was 7.9 at a CO<sub>2</sub> concentration of 14.5 vol % and testing pressure of 5 bar. The results of the mixed gas separation analysis indicate that the fabricated composite membrane can be considered as a viable alternative membrane material for gas separation processes.

**Author Contributions:** S.Z.: Formal analysis, investigation, data curation, writing—original draft, visualization. Y.F.Y.: Conceptualization, methodology, validation, resources, writing—review and editing, supervision, funding acquisition, project administration. N.J.: Conceptualization, methodology, resources, supervision. L.S.T.: Supervision. All authors have read and agreed to the published version of the manuscript.

**Funding:** This research was funded by Yayasan Universiti Teknologi PETRONAS] YUTP Grant (Cost Center: 015LC0-099).

**Institutional Review Board Statement:** Not applicable.

**Informed Consent Statement:** Not applicable.

**Data Availability Statement:** Not applicable.

**Acknowledgments:** The financial and technical supports provided by the Yayasan Universiti Teknologi PETRONAS (YUTP) Research Grant and the CO<sub>2</sub> Research Centre, Universiti Teknologi PETRONAS, are duly acknowledged.

**Conflicts of Interest:** The authors declare no conflict of interest.

#### References

1. Shah, M.S.; Tsapatsis, M.; Siepmann, J.I. Hydrogen Sulfide Capture: From Absorption in Polar Liquids to Oxide, Zeolite, and Metal–Organic Framework Adsorbents and Membranes. *Chem. Rev.* **2017**, *117*, 9755–9803. [[CrossRef](#)] [[PubMed](#)]
2. Mazyan, W.; Ahmadi, A.; Ahmed, H.; Hoorfar, M. Market and technology assessment of natural gas processing: A review. *J. Nat. Gas Sci. Eng.* **2016**, *30*, 487–514. [[CrossRef](#)]
3. Baker, R.W. and K.L. Natural Gas Processing with Membranes: An Overview. *Ind. Eng. Chem. Res.* **2008**, *47*, 2109–2121. [[CrossRef](#)]
4. Washim Uddin, M.; Hägg, M.-B. Natural gas sweetening—The effect on CO<sub>2</sub>–CH<sub>4</sub> separation after exposing a facilitated transport membrane to hydrogen sulfide and higher hydrocarbons. *J. Membr. Sci.* **2012**, *423–424*, 143–149. [[CrossRef](#)]
5. Liu, G.; Chernikova, V.; Liu, Y.; Zhang, K.; Belmabkhout, Y.; Shekhah, O.; Zhang, C.; Yi, S.; Eddaoudi, M.; Koros, W.J. Mixed matrix formulations with MOF molecular sieving for key energy-intensive separations. *Nat. Mater.* **2018**, *17*, 283–289. [[CrossRef](#)]

6. Koronful, N.; Peters, K.; Ali, M.F.; Skulsangjuntr, J.; Jiang, L.; Kleine, A.; Basu, D.; Bencomo, J.; Hernandez, J.; Brink, G. Carbon Dioxide in Reservoir Gases: New Insights from Basin and Petroleum System Modeling. In *SPE Asia Pacific Oil and Gas Conference and Exhibition*; OnePetro: London, UK, 2018; Volume 1, p. 3121. [\[CrossRef\]](#)
7. Choi, Y.-S.; Nešić, S. Determining the corrosive potential of CO<sub>2</sub> transport pipeline in high pCO<sub>2</sub>–water environments. *Int. J. Greenh. Gas Control* **2011**, *5*, 788–797. [\[CrossRef\]](#)
8. Zornoza, B.; Martinez-Joaristi, A.; Serra-Crespo, P.; Tellez, C.; Coronas, J.; Gascon, J.; Kapteijn, F. Functionalized flexible MOFs as fillers in mixed matrix membranes for highly selective separation of CO<sub>2</sub> from CH<sub>4</sub> at elevated pressures. *Chem. Commun.* **2011**, *47*, 9522–9524. [\[CrossRef\]](#)
9. Khan, I.U.; Othman, M.H.D.; Jilani, A.; Ismail, A.F.; Hashim, H.; Jaafar, J.; Zulkhairun, A.K.; Rahman, M.A.; Rehman, G.U. ZIF-8 based polysulfone hollow fiber membranes for natural gas purification. *Polym. Test.* **2020**, *84*, 106415. [\[CrossRef\]](#)
10. Robeson, L.M. The upper bound revisited. *J. Membr. Sci.* **2008**, *320*, 390–400. [\[CrossRef\]](#)
11. Suleman, M.S.; Lau, K.K.; Yeong, Y.F. Development, characterization and performance evaluation of a swelling resistant membrane for CO<sub>2</sub>/CH<sub>4</sub> separation. *J. Nat. Gas Sci. Eng.* **2018**, *52*, 390–400. [\[CrossRef\]](#)
12. Ismail, A.F.; Lorna, W. Suppression of plasticization in polysulfone membranes for gas separations by heat-treatment technique. *Sep. Purif. Technol.* **2003**, *30*, 37–46. [\[CrossRef\]](#)
13. Roslan, R.A.; Lau, W.J.; Sakthivel, D.B.; Khademi, S.; Zulkhairun, A.K.; Goh, P.S.; Ismail, A.F.; Chong, K.C.; Lai, S.O. Separation of CO<sub>2</sub>/CH<sub>4</sub> and O<sub>2</sub>/N<sub>2</sub> by polysulfone hollow fiber membranes: Effects of membrane support properties and surface coating materials. *J. Polym. Eng.* **2018**, *38*, 871–880. [\[CrossRef\]](#)
14. Zulkhairun, A.K.; Fachrurrazi, Z.G.; Nur Izwanne, M.; Ismail, A.F. Asymmetric hollow fiber membrane coated with polydimethylsiloxane–metal organic framework hybrid layer for gas separation. *Sep. Purif. Technol.* **2015**, *146*, 85–93. [\[CrossRef\]](#)
15. Li, T.; Pan, Y.; Peinemann, K.-V.; Lai, Z. Carbon dioxide selective mixed matrix composite membrane containing ZIF-7 nano-fillers. *J. Membr. Sci.* **2013**, *425–426*, 235–242. [\[CrossRef\]](#)
16. Lin, H.; Freeman, B.D. Materials selection guidelines for membranes that remove CO<sub>2</sub> from gas mixtures. *J. Mol. Struct.* **2005**, *739*, 57–74. [\[CrossRef\]](#)
17. Li, G.; Kujawski, W.; Válek, R.; Koter, S. A review-The development of hollow fibre membranes for gas separation processes. *Int. J. Greenh. Gas Control* **2021**, *104*, 103195. [\[CrossRef\]](#)
18. Chung, T.S. Calculation of the intrusion depth and its effects on microporous composite membranes. *Sep. Purif. Technol.* **1997**, *12*, 17–23. [\[CrossRef\]](#)
19. Yang, H.-C.; Hou, J.; Chen, V.; Xu, Z.-K. Surface and interface engineering for organic–inorganic composite membranes. *J. Mater. Chem. A* **2016**, *4*, 9716–9729. [\[CrossRef\]](#)
20. Chen, H.Z.; Thong, Z.; Li, P.; Chung, T.-S. High performance composite hollow fiber membranes for CO<sub>2</sub>/H<sub>2</sub> and CO<sub>2</sub>/N<sub>2</sub> separation. *Int. J. Hydrogen Energy* **2014**, *39*, 5043–5053. [\[CrossRef\]](#)
21. Liu, S.L.; Shao, L.; Chua, M.L.; Lau, C.H.; Wang, H.; Quan, S. Recent progress in the design of advanced PEO-containing membranes for CO<sub>2</sub> removal. *Prog. Polym. Sci.* **2013**, *38*, 1089–1120. [\[CrossRef\]](#)
22. Sutrisna, P.D.; Hou, J.; Li, H.; Zhang, Y.; Chen, V. Improved operational stability of Pebax-based gas separation membranes with ZIF-8: A comparative study of flat sheet and composite hollow fibre membranes. *J. Membr. Sci.* **2017**, *524*, 266–279. [\[CrossRef\]](#)
23. Suhaimi, N.H.; Yeong, Y.F.; Jusoh, N.; Chew, T.L.; Bustam, M.A.; Suleman, S. Separation of CO<sub>2</sub> from CH<sub>4</sub> using mixed matrix membranes incorporated with amine functionalized MIL-125 (Ti) nanofiller. *Chem. Eng. Res. Des.* **2020**, *159*, 236–247. [\[CrossRef\]](#)
24. Waqas Anjum, M.; Bueken, B.; De Vos, D.; Vankelecom, I.F.J. MIL-125(Ti) based mixed matrix membranes for CO<sub>2</sub> separation from CH<sub>4</sub> and N<sub>2</sub>. *J. Membr. Sci.* **2016**, *502*, 21–28. [\[CrossRef\]](#)
25. Zakariya, S.; Yeong, Y.F.; Jusoh, N.; Tan, L.S. Fabrication of multilayer composite hollow fiber membrane comprising NH<sub>2</sub>-MIL-125 (Ti) for CO<sub>2</sub> removal from CH<sub>4</sub>. *Mater. Today Proc.* **2021**. Peerreview. [\[CrossRef\]](#)
26. Brunetti, A.; Tocci, E.; Cersosimo, M.; Kim, J.S.; Lee, W.H.; Seong, J.G.; Lee, Y.M.; Drioli, E.; Barbieri, G. Mutual influence of mixed-gas permeation in thermally rearranged poly(benzoxazole-co-imide) polymer membranes. *J. Membr. Sci.* **2019**, *580*, 202–213. [\[CrossRef\]](#)
27. Sánchez-Laínez, J.; Gracia-Guillén, I.; Zornoza, B.; Téllez, C.; Coronas, J. Thin supported MOF based mixed matrix membranes of Pebax<sup>®</sup> 1657 for biogas upgrade. *New J. Chem.* **2019**, *43*, 312–319. [\[CrossRef\]](#)
28. Sridhar, S.; Bee, S.; Bhargava, S. Membrane-based Gas Separation: Principle, Applications and Future Potential. *Chem. Eng. Dig.* **2014**, *2014*.
29. Mubashir, M.; Yeong, Y.F.; Chew, T.L.; Lau, K.K. Optimization of spinning parameters on the fabrication of NH<sub>2</sub>-MIL-53(Al)/cellulose acetate (CA) hollow fiber mixed matrix membrane for CO<sub>2</sub> separation. *Sep. Purif. Technol.* **2019**, *215*, 32–43. [\[CrossRef\]](#)
30. Jusoh, N.; Lau, K.K.; Shariff, A.M.; Yeong, Y.F. Capture of bulk CO<sub>2</sub> from methane with the presence of heavy hydrocarbon using membrane process. *Int. J. Greenh. Gas Control* **2014**, *22*, 213–222. [\[CrossRef\]](#)
31. Genduso, G.; Wang, Y.; Ghanem, B.; Pinnau, I. Permeation, sorption, and diffusion of CO<sub>2</sub>-CH<sub>4</sub> mixtures in polymers of intrinsic microporosity: The effect of intrachain rigidity on plasticization resistance. *J. Membr. Sci.* **2019**, *584*, 100–109. [\[CrossRef\]](#)
32. Jusoh, N.; Yeong, Y.F.; Lau, K.K.; Shariff, A.M. Fabrication of silanated zeolite T/6FDA-durene composite membranes for CO<sub>2</sub>/CH<sub>4</sub> separation. *J. Clean. Prod.* **2017**, *166*, 1043–1058. [\[CrossRef\]](#)

33. Khanbabaee, G.; Aalaei, J.; Rahmatpour, A. Polymeric Nanocomposite Membranes for Gas Separation. *Sustain. Membr. Technol. Energy Water Environ.* **2012**, *87*–94. Available online: [https://books.google.com.hk/books?hl=en&lr=&id=-56-IsIkeLsC&oi=fnd&pg=PA87&dq=Polymeric+Nanocomposite+Membranes+for+Gas+Separation.&ots=sKS8HMdjf2&sig=8pJtM5skDGgZlfEBDsAjqI8q3kl&redir\\_esc=y&hl=zh-CN&sourceid=cndr#v=onepage&q=Polymeric%20Nanocomposite%20Membranes%20for%20Gas%20Separation.&f=false](https://books.google.com.hk/books?hl=en&lr=&id=-56-IsIkeLsC&oi=fnd&pg=PA87&dq=Polymeric+Nanocomposite+Membranes+for+Gas+Separation.&ots=sKS8HMdjf2&sig=8pJtM5skDGgZlfEBDsAjqI8q3kl&redir_esc=y&hl=zh-CN&sourceid=cndr#v=onepage&q=Polymeric%20Nanocomposite%20Membranes%20for%20Gas%20Separation.&f=false) (accessed on 10 February 2022).
34. Ghasemi Estahbanati, E.; Omidkhah, M.; Ebadi Amooghin, A. Interfacial Design of Ternary Mixed Matrix Membranes Containing Pebax 1657/Silver-Nanopowder/[BMIM][BF<sub>4</sub>] for Improved CO<sub>2</sub> Separation Performance. *ACS Appl. Mater. Interfaces* **2017**, *9*, 10094–10105. [[CrossRef](#)]
35. Bharali, P.; Borthakur, S.; Hazarika, S. Selective Permeation of CO<sub>2</sub> through Amine Bearing Facilitated Transport Membranes. *J. Membr. Sci. Technol.* **2020**, *203*. [[CrossRef](#)]
36. Gong, X.-Y.; Huang, Z.-H.; Zhang, H.; Liu, W.-L.; Ma, X.-H.; Xu, Z.-L.; Tang, C.Y. Novel high-flux positively charged composite membrane incorporating titanium-based MOFs for heavy metal removal. *Chem. Eng. J.* **2020**, *398*, 125706. [[CrossRef](#)]
37. Zhu, X.; Yu, Z.; Liu, Y.; Li, X.; Long, R.; Wang, P.; Wang, J. NH<sub>2</sub>-MIL-125@PAA composite membrane for separation of oil/water emulsions and dyes. *Colloids Surfaces A Physicochem. Eng. Asp.* **2021**, *630*, 127542. [[CrossRef](#)]
38. Wang, M.; Yang, L.; Yuan, J.; He, L.; Song, Y.; Zhang, H.; Zhang, Z.; Fang, S. Heterostructured Bi<sub>2</sub>S<sub>3</sub>@NH<sub>2</sub>-MIL-125(Ti) nanocomposite as a bifunctional photocatalyst for Cr(vi) reduction and rhodamine B degradation under visible light. *RSC Adv.* **2018**, *8*, 12459–12470. [[CrossRef](#)]
39. Yin, S.; Chen, Y.; Li, M.; Hu, Q.; Ding, Y.; Shao, Y.; Di, J.; Xia, J.; Li, H. Construction of NH<sub>2</sub>-MIL-125(Ti)/Bi<sub>2</sub>WO<sub>6</sub> composites with accelerated charge separation for degradation of organic contaminants under visible light irradiation. *Green Energy Environ.* **2020**, *5*, 203–213. [[CrossRef](#)]
40. Yang, J.; Zhou, Q.; Shen, K.; Song, N.; Ni, L. Controlling nanodomain morphology of epoxy thermosets templated by poly(caprolactone)-block-poly(dimethylsiloxane)-block-poly(caprolactone) ABA triblock copolymer. *RSC Adv.* **2018**, *8*, 3705–3715. [[CrossRef](#)]
41. Yuan, F.; Wang, Z.; Li, S.; Wang, J.; Wang, S. Formation–structure–performance correlation of thin film composite membranes prepared by interfacial polymerization for gas separation. *J. Membr. Sci.* **2012**, *421–422*, 327–341. [[CrossRef](#)]
42. Shen, J.; Liu, G.; Huang, K.; Li, Q.; Guan, K.; Li, Y.; Jin, W. UiO-66-polyether block amide mixed matrix membranes for CO<sub>2</sub> separation. *J. Membr. Sci.* **2016**, *513*, 155–165. [[CrossRef](#)]
43. Sanaeepur, H.; Ahmadi, R.; Sinaei, M.; Kargari, A. Pebax-Modified Cellulose Acetate Membrane for CO<sub>2</sub>/N<sub>2</sub> Separation. *J. Membr. Sci. Res.* **2019**, *5*, 25–32. [[CrossRef](#)]
44. Lee, M.-S.; Park, M.; Kim, H.; Park, S.-J. Effects of Microporosity and Surface Chemistry on Separation Performances of N-Containing Pitch-Based Activated Carbons for CO<sub>2</sub>/N<sub>2</sub> Binary Mixture. *Sci. Rep.* **2016**, *6*, 23224. [[CrossRef](#)]
45. Halim, M.; Kadirkhan, F.; Mustapa, W.; Soh, W.K.; Yeo, S. Natural gas sweetening polymeric membrane: Established optimum operating condition at 70% of CO<sub>2</sub> concentration feed gas stream. *Malays. J. Fundam. Appl. Sci.* **2020**, *16*, 54–58. [[CrossRef](#)]
46. Ismail, A.F.; Yaacob, N. Performance of treated and untreated asymmetric polysulfone hollow fiber membrane in series and cascade module configurations for CO<sub>2</sub>/CH<sub>4</sub> gas separation system. *J. Membr. Sci.* **2006**, *275*, 151–165. [[CrossRef](#)]
47. Falbo, F.; Brunetti, A.; Barbieri, G.; Drioli, E.; Tasselli, F. CO<sub>2</sub>/CH<sub>4</sub> separation by means of Matrimid hollow fibre membranes. *Appl. Petrochem. Res.* **2016**, *6*, 439–450. [[CrossRef](#)]
48. Zhang, Y.; Musselman, I.H.; Ferraris, J.P.; Balkus, K.J. Gas permeability properties of Matrimid<sup>®</sup> membranes containing the metal-organic framework Cu-BPY-HFS. *J. Membr. Sci.* **2008**, *313*, 170–181. [[CrossRef](#)]
49. Li, X.; Jiang, Z.; Wu, Y.; Zhang, H.; Cheng, Y.; Guo, R.; Wu, H. High-performance composite membranes incorporated with carboxylic acid nanogels for CO<sub>2</sub> separation. *J. Membr. Sci.* **2015**, *495*, 72–80. [[CrossRef](#)]
50. Rios, R.; Stragliotto, F.; Peixoto, H.; Torres, A.; Bastos-Neto, M.; Azevedo, D.; Cavalcante, C., Jr. Studies on the adsorption behavior of CO<sub>2</sub>-CH<sub>4</sub> mixtures using activated carbon. *Braz. J. Chem. Eng.* **2013**, *30*, 939–951. [[CrossRef](#)]
51. Wang, S.-E.; Huang, Y.; Hu, K.; Tian, J.; Zhao, S. A highly sensitive and selective aptasensor based on fluorescence polarization for the rapid determination of oncoprotein vascular endothelial growth factor (VEGF). *Anal. Methods* **2014**, *6*, 62–66. [[CrossRef](#)]